Current distribution inside Py/Cu lateral spin-valve devices

J. Hamrle,[1,2] T. Kimura,[1,2] Y. Otani,[1,2,3] K. Tsukagoshi,[4] and Y. Aoyagi[4]
[1]*FRS, The Institute of Physical and Chemical Research (RIKEN), 2-1 Hirosawa, Wako, Saitama 351-0198, Japan*
[2]*CREST, Japan Science & Technology Corporation, Japan*
[3]*ISSP, University of Tokyo, Kashiwa-shi, Chiba 277-8581, Japan*
[4]*RIKEN, 2-1 Hirosawa, Wako, Saitama 351-0198, Japan*
(Received 15 July 2004; revised manuscript received 11 October 2004; published 4 March 2005)

We have investigated experimentally the nonlocal voltage signal (NLVS) in the lateral Permalloy (Py)/Cu/Py spin-valve devices with different width of Cu stripes. We found that NLVS strongly depends on the distribution of the spin-polarized current inside Cu strip in the vicinity of the Py detector. To explain these data we have developed a diffusion model describing spatial (three dimensional) distribution of the spin-polarized current in the device. The results of our calculations show that NLVS is decreased by a factor of 10 due to spin flip scattering occurring at the Py/Cu interface. The interface resistivity on the Py/Cu interface is also present, but its contribution to reduction of NLVS is minor. We also found that most of the spin-polarized current is injected within the region 30 nm from the Py injector/Cu interface. In the area at Py detector/Cu interface, the spin-polarized current is found to flow mainly close on the injector side, with $1/e$ exponential decay in the magnitude within the distance 80 nm.

DOI: 10.1103/PhysRevB.71.094402 PACS number(s): 75.75.+a, 85.70.Ay, 85.70.Kh

I. INTRODUCTION

Spintronics is a quickly evolving field providing the possibility of manipulating spin degrees of freedom in the solid state systems.[1,2] Spin injection, transport, and detection in metals and semiconductors are of particular importance to construct effective spintronic devices such as a spin battery[3] and spin torque transistor,[4] etc. Such devices have great advantages over the conventional electronic devices because of additional spin functionalities. To realize the device it is key to obtain both large spin-polarized current and spin accumulation. It is also important to understand the diffusive nature of the spin-polarized currents in multiterminal devices.

The pioneering experimental and theoretical works concerning nonlocal devices were carried out by Johnson[5,6] and Fert and Lee,[7] respectively. Recently, the lateral nonlocal device was proposed by Jedema *et al.*[8–10] They succeeded in detecting the clear spin-accumulation signal in the vicinity of the nonmagnetic (N)/ferromagnetic (F) planar junction by the nonlocal voltage signal (NLVS) even at room temperature.[9,10] The nonlocal technique allows one to extract only spin-polarized current contribution from the spin-dependent phenomena and to reduce spurious effects such as Hall effect and anisotropic magnetoresistance. Furthermore, it maybe useful to induce spin-injection magnetization reversal[11] without the charge current, leading to the solution for the energy dissipation problem due to Joule heat.

Here, we study experimentally the distribution of the spin-polarized current in nonlocal configuration. So far, the spin-polarized current transport is analytically investigated using the one-dimensional (1D) Boltzmann diffusion model.[9,12–15] As these models predict too large NLVS, we have developed formalism to calculate spatial three-dimensional (3D) distribution of spin-polarized current. However, large decrease of NLVS cannot be attributed to spatial distribution of spin-polarized current, and we attribute it to spin scattering at the Py/Cu interface.

II. DEVICE PREPARATION AND EXPERIMENTAL RESULTS

We fabricated lateral spin-valve devices consisting of two Py wires bridged by a Cu strip by means of nanofabrication techniques. Figure 1 shows a scanning electron microscope (SEM) image for one of the fabricated devices. First, we fabricated both Py wires of width $w_{\mathrm{Py}}=120$ nm and of thickness $t_{\mathrm{Py}}=20$ nm with the spacing of $\ell_{\mathrm{Cu}}=170$ nm by electron-beam lithography and lift-off technique. Py layer was evaporated by an electron-beam gun at 2×10^{-8} Torr. Ends of the first Py wire are connected to large pads pattern for assisting the nucleation of the domain wall, although the ends of the second one are flat-end shaped. Hence, each Py wire has a different switching field.

Both Py wires are bridged by Cu strip of thickness $t_{\mathrm{Cu}}=80$ nm, having widths $w_{\mathrm{Cu}}=100$, 300, and 500 nm for three different devices. Prior to Cu deposition, the Py surface was cleaned by Ar^{+} bombardment and then the sample was shortly taken out of vacuum to change the vacuum chamber. Then Cu was evaporated by resistance heating. The contact resistance of the interface was found ohmic and very low indicating a transparent contact. The conductivity of Cu is $\sigma_{\mathrm{Cu,RT}}=48.1\times10^{6}\ \Omega^{-1}\,\mathrm{m}^{-1}$, $\sigma_{\mathrm{Cu,4\ K}}=131\times10^{6}\ \Omega^{-1}\,\mathrm{m}^{-1}$ at room temperature, 4 K, respectively.

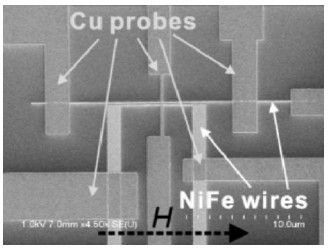

FIG. 1. SEM image of the fabricated lateral spin-valve device.

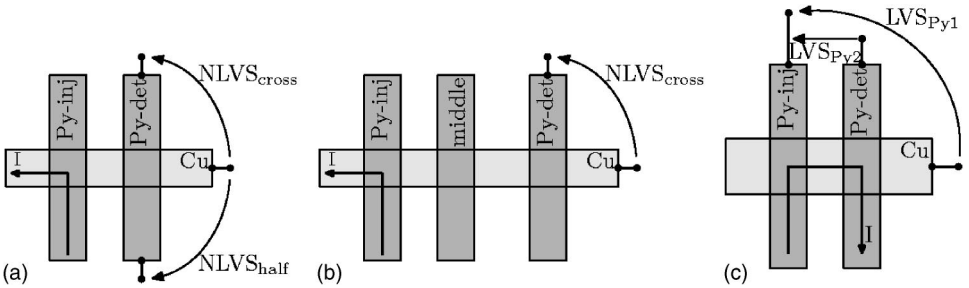

FIG. 2. NLVS for system with (a) two wires and (b) with three wires. (c) *Local* voltage signal (LVS) for system with two wires.

Notice that the present Cu strip has smaller residual resistivity than that of Jedema *et al.*[9] The NLVS measurements were performed at room temperature with the magnetic field applied parallel along the Py wires.

NLVS measurements were performed using a standard current-bias lock-in technique at room temperature. We measured the NLVS as a function of external magnetic field by using two different probe configurations, called "half" and "cross." The difference between both configurations is whether the current and voltage probes are located on the same side or not as sketched in Figs. 2(a) or 3(a). The one-dimensional (1D) diffusion model[15,16] predicts that the obtained NLVS should be the same. However, as the spin-polarized current has the spatial distribution, the NLVS shows the difference between both probe configurations.

Figures 3(c) and 3(e) show a NLVS for $w_{Cu}=100$ nm with half and cross probe configuration, respectively. The obtained difference of NLVS between parallel and antiparallel magnetization (DNLVS) is 0.7 and 0.6 mΩ at room temperature, respectively. Figures 3(d) and 3(f) show NLVS for $w_{Cu}=500$ nm with half and cross configurations, providing 0.6 and 0.1 mΩ, respectively.

Experimental values of DNLVS as a function of w_{Cu} are presented in Fig. 4(a). Experimental data show that the difference between cross and half in DNLVS increases with increasing w_{Cu}.

The other parameters (at room temperature) used in our calculations are as follows: Py conductivity $\sigma_{Py}=7.3\times10^6\ \Omega^{-1}\,m^{-1}$, Py bulk spin asymmetry coefficient $\beta=0.7$ ($\sigma_{\uparrow,Py}=\sigma_{Py}(1+\beta)/2$, $\sigma_{\downarrow,Py}=\sigma_{Py}(1-\beta)/2$) (Refs. 17–19), spin-flip lengths $\lambda_{Py}=4.3$ nm (Ref. 17) and $\lambda_{Cu}=350$ nm (Ref. 16).

III. EXPERIMENT VERSUS THEORY

A. 1D treatment

In the literature, there are two models describing NLVS (and DNLVS) inside a metallic lateral spin-valve device: one given by Jedema *et al.*[16] and the other by Takahashi and Maekawa.[15] Both models approximate the device into 1D wire circuit, in which the propagation of electrochemical potential $\mu_{\uparrow/\downarrow}$ and spin-polarized current $J_{\uparrow/\downarrow}$ is described by the standard Valet-Fert model.[13] At an intersection point of sev-

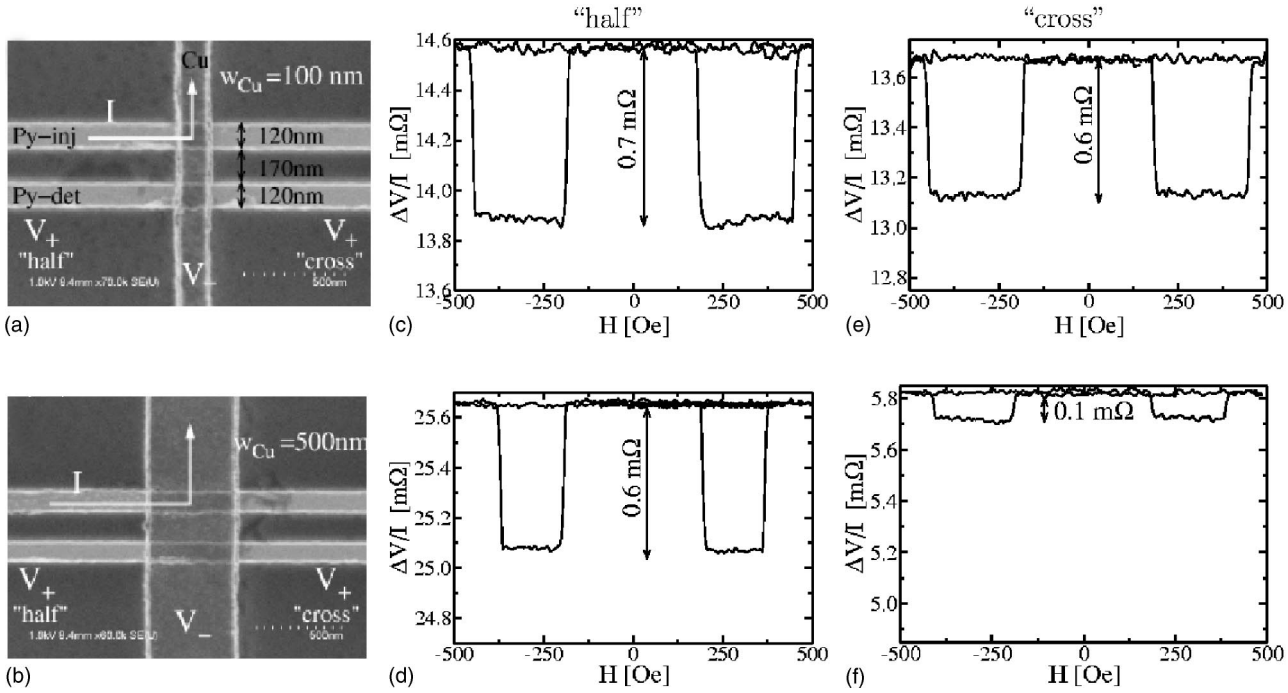

FIG. 3. (a) and (b) SEM image of a detail of the lateral spin-valve device with $w_{Cu}=100,500$ nm, respectively, with sketched current flows and cross and half detection configuration. (c–f) NLVS as a function of external magnetic field, obtained for cross and half configuration for $w_{Cu}=100,500$ nm.

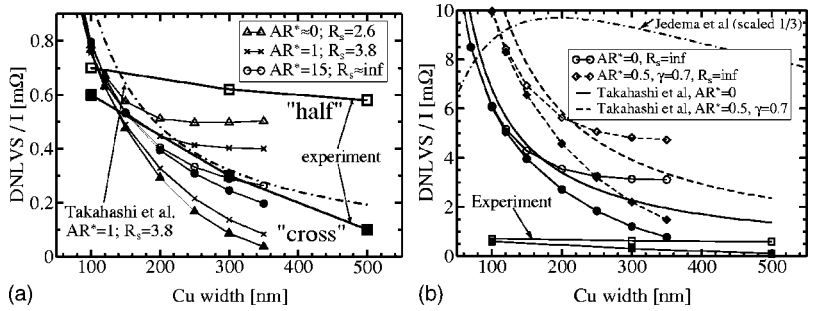

FIG. 4. (a) and (b) Experimental values of DNLVS in both half (empty squares) and cross (solid squares) configuration as a function of Cu wire width w_{Cu}. These data are compared with (i) 1D models (lines without symbols), namely Jedema, Eq. (2), and Takahashi, Eq. (3) (see Sec. III A), (ii) 3D models (symbols) (see Sec. III B 2). The DNLVS is calculated for transparent interface ($AR^*=0$, $AR_s=\mathrm{inf}$), for interface with interface resistivity ($AR^*=0.5, \gamma=0.7, AR_s=\mathrm{inf}$) and for case with both interface resistivity and spin-filp resistance ($AR^*=\{0,1,15\}, AR_s=\{2.6,3.8,\mathrm{inf}\}, \gamma=0$). AR^* and AR_s are interface and surface scattering resistances for Py/Cu interface, units in $\mathrm{f}\Omega\mathrm{m}^2$.

eral wires (hereafter called node), e.g., intersection of Cu and Py wires, the boundary conditions, expressed as generalized Kirchoff's laws, are

$$\sum_n J_{n,\uparrow/\downarrow} = 0,$$

$$\mu_{n,\uparrow/\downarrow} = \mathrm{const}_{\uparrow/\downarrow}, \tag{1}$$

where n is an index of all the wires connected to a given node. Hence, the $\mu_{\uparrow/\downarrow}$ (which can be understand as a voltage here) is the same for each 1D wire attached to a given node, and $J_{\uparrow/\downarrow}$ is conserved while flowing through each node.

The model of Jedema *et al.*[16] has two assumptions, which are not fulfilled in our case of the Py/Cu device: (a) they assume cross-sectional areas of all the wires in the device were the same (i.e., they considered more continuity of up and down current densities $j_{\uparrow/\downarrow}$ than up and down currents $J_{\uparrow/\downarrow}$ at each node) and (b) they assume $(\lambda_F,\lambda_N) \gg (w_F,w_N)$, where (w_F,w_N) are widths of F, N wires, respectively. Assuming transparent F/N interface, this model predicts DNLVS in form [from Eq. (12) in Ref. 16]

$$\mathrm{DNLVS}_{\mathrm{Jedema}} = \frac{\beta^2 R_N \exp[-\ell_N/(2\lambda_N)]}{\left(\frac{R_N}{R_F}+1\right)\left\{\frac{R_N}{R_F}\sinh[\ell_N/(2\lambda_N)]+\cosh[\ell_N/(2\lambda_N)]\right\}}, \tag{2}$$

where $R_N=\lambda_N/(\sigma_N S_N)$, $R_F=\lambda_F/(\sigma_F S_F(1-\beta^2))$ are characteristic spin-flip resistances of N, F materials, respectively and ℓ_N in separating distance between both F wires. The comparison of DNLVS obtained from this model (when extended to the case for different cross-sectional areas of wires) with our experimental data is shown on Fig. 4(b) (dashed-dotted line), showing that this model predicts about $40\times$ large value than the experimental one.

These drawbacks were partly overcome by Takahashi and Maekawa,[15] assuming that (a) $\lambda_F \ll (w_F,w_N) \ll \lambda_N$ and (b) that current at the F/N interface is homogeneous. Later we will show that assumption (b) is not correct for ohmic junctions, but is correct for tunnel junctions. Although they derived their model from basic equations, the same results can be obtained when both F injector and F detector, attached to the N wire, are described by the 1D model, where F wires have an effective cross-section area as of Py/Cu interface, i.e., in our case $\tilde{S}_F=w_F w_N$. The DNLVS calculated from this model is presented in Fig. 4(b) (solid line) for the case with interface resistance $AR^*_{\mathrm{Py/Cu}}=0$ and $AR^*_{\mathrm{Py/Cu}}=0.5\ \mathrm{f}\Omega\,\mathrm{m}^2$, $\gamma=0.7$ (Ref. 18) (dashed line). Note that $AR^{\uparrow}_{\mathrm{Py/Cu}}=2AR^*_{\mathrm{Py/Cu}}(1-\gamma)$, $AR^{\downarrow}_{\mathrm{Py/Cu}}=2AR^*_{\mathrm{Py/Cu}}(1+\gamma)$. This 1D model describes quite well the experimentally observed DNLVS but gives about ten times larger magnitude than the experimental results. When assuming transparent interface, $AR^*_{\mathrm{Py/Cu}}=0$, the analytical expression of DNLVS is [from Eq. (3) in Ref. 15]

$$\mathrm{DNLVS}_{\mathrm{Takahashi}} = \frac{4\beta^2 R_N \exp[-\ell_N/\lambda_N]}{\left(\frac{R_N}{R_F}+2\right)^2-\left(\frac{R_N}{R_F}\right)^2\exp[-2\ell_N/\lambda_N]}. \tag{3}$$

The case of the Takahashi model incorporating spin-flip interface resistance $AR_{s,\mathrm{Py/Cu}}$ (discussed in detail later in Sec. III B 2) was not calculated by formulas, but by means of our theory of electrical circuit of 1D spin-dependent-resistance elements (SDRE).[20]

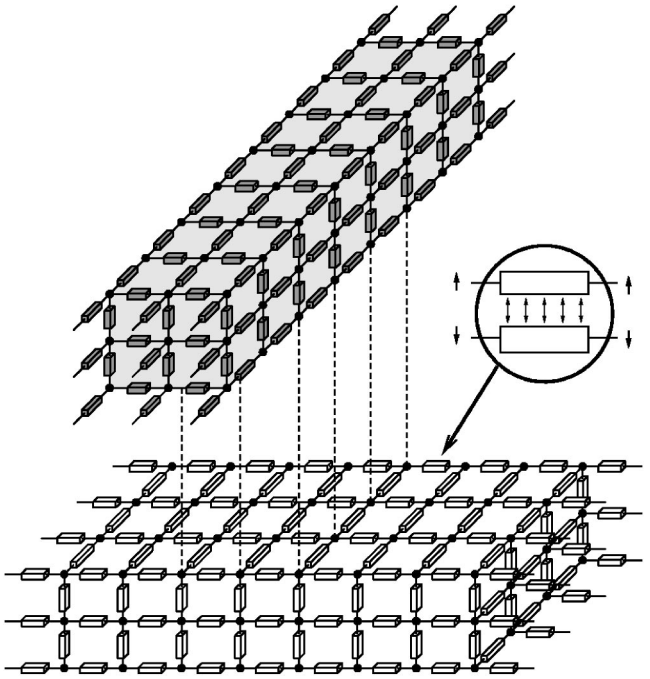

FIG. 5. The sketch of 3D circuit of spin-dependent-resistance elements (SDRE). Circle inset sketches that each SDRE consists of spin-up and spin-down resistances and of the shunting resistors between up and down channels. Note that each node and wire on the sketch represents a "bus" containing spin-up and spin-down channels.

B. 3D treatment

In order to understand the spin-polarized currents inside the device in detail, we have developed a model calculating 3D distribution of $\mu_{\uparrow/\downarrow}$ and spin-polarized current density $j_{\uparrow/\downarrow}$ inside the device.[20] Our model is based on the 3D electrical circuit of SDRE (Fig. 5). The response of each SDRE is determined by 1D models.[13,16] As sketched in the inset of Fig. 5, each SDRE consists of resistance for spin-up, spin-down channels and spin-flip resistance shunting up and down channels. This shunting resistance can be regarded as the "probability" that electron spins are flipped when passing SDRE. Boundary conditions at each node connecting SDRE are given by Eq. (1).

In this model we can also account surface or interface resistance (scattering), AR_{ss} or AR_s, respectively, short-cutting up and down channels at the surface or interface. For a detailed description of the formalism please see Ref. 20.

1. Test for the 3D diffusion model

To estimate precision of our 3D calculations, we have calculated $j_{\uparrow/\downarrow}$, $\mu_{\uparrow/\downarrow}$ and magnetoresistivity ratio (MR) in Cu/Py(20)/Cu(20)/Py(20)/Cu *multilayer* structure (dimensions in nm) using different grid sizes for Py. The results of these calculations should be identical with the 1D Valet-Fert model.[13] We investigate the calculation precision only with the grid size of Py, as $\lambda_{Py} \ll \lambda_{Cu}$.

Figure 6 shows the profile of spin-polarized current $j_{sp} = j_\uparrow - j_\downarrow$ through the antiparallel Py/Cu multilayer structure. The used lateral grid size (i.e., grid distances parallel with Py/Cu interfaces) is 10 nm, perpendicular grid (i.e., grid perpendicular to interfaces) is 1, 5, 10 nm, giving j_{sp} precision inside Py being 4%, 9%, 15%, respectively. Three-dimensional calculations give a larger value of MR by 8%, 16%, 33% than a 1D calculation. For in-plane grid size 5 nm, the MR is larger by 4%, 11%, 26%. It shows that (i) with decrease of grid size, j_{sp} and MR converge to correct values and (ii) the small perpendicular grid size is more important than the in-plane one.

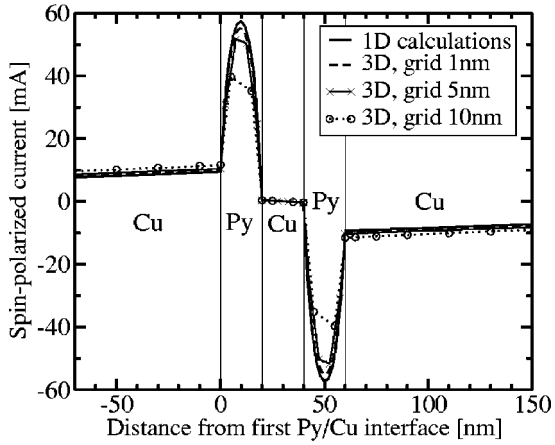

FIG. 6. The profile of $j_{sp} = j_\uparrow - j_\downarrow$ through Cu/Py(20)/Cu(20)/Py(20)/Cu pillar structure, dimensions in nm, calculated for 1D VF model (full line) and compared with our 3D calculations with perpendicular-to-interface grid size 1, 5, and 10 nm. Lateral (parallel-to-interface) grid size is 10 nm.

Figure 7 shows a dependence of DNLVS in the lateral spin-valve structure on various lateral (i.e., parallel with substrate surface) grid sizes. The simulated device is different than the real one; two Py wires 15 nm thick and 50 nm wide are separated by a distance of 80 nm and bridged by a 55-nm-thick, 50-nm-wide Cu strip.

DNLVS has been calculated for perpendicular grid size 5 nm (square in Fig. 7) and 2.5 nm (diamond), providing larger DNLVS by 18%, 11%, respectively, with respect to the converged DNLVS value. In both cases, larger grid size leads to larger DNLVS.

In all simulations of real structure, we used perpendicular grid size 5 nm, lateral grid size 10 nm and, in the vicinity of

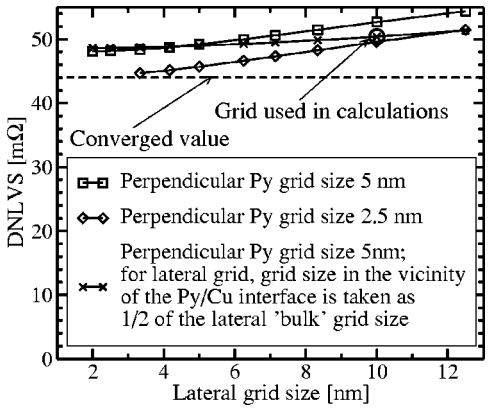

FIG. 7. Dependence of DNLVS on lateral grid size. Details in Sec. III B 1.

the Py/Cu interface, lateral grid size 5 nm. This grid configuration is denoted by a circle on the Fig. 7, providing agreement with DNLVS converged value of 13%, in agreement with the above discussion. Unfortunately, in our calculations, we cannot use a smaller grid size due to numerical limitations. We conclude that (i) the precision of our 3D calculations is about 20% and (ii) calculated DNLVS has a tendency to be overestimated.

2. 3D calculations of DNLVS

Figure 4(b) presents DNLVS calculated from the 3D model for $AR^*_{Py/Cu}=0$ (circle) and for $AR^*_{Py/Cu}=0.5\ f\Omega\ m^2$, $\gamma=0.7$ (Ref. 18) (diamond). Both DNLVS have about the same shape and slightly smaller magnitude compared to values from the 1D model by Takahashi and Maekawa [15] (solid and dashed lines without symbols). In agreement with the experiment, for larger w_{Cu}, the DNLVS has different values in half and cross configuration, reflecting inhomogeneous j_{sp} at the position of the detector. As will be shown in Sec. IV, the j_{sp} is also strongly inhomogeneous at the injector position. However, the approximative agreement between 3D models and 1D models shows that the influence of inhomogeneous current injection is not very important to the magnitude of DNLVS. As our 3D models tend to overestimate DNLVS, we conclude that inhomogeneous current injection decreases DNLVS, but only about 20%.

Both 1D and 3D models show that the presence of $R^*_{Py/Cu}$ together with large positive value of γ increases DNLVS. When $R^*_{Py/Cu}>0$, $\gamma=0$, DNLVS decreases. It may be possible that $\gamma>0$, but this contribution to DNLVS is smeared by other contributions decreasing DNLVS. Therefore, in the following we assume $\gamma=0$.

Now, let us discuss which mechanism decreases DNLVS. To be more sure with analysis, we take into account more experimental data (which are going to be published elsewhere[21]) on two different samples, fabricated exactly the same way as the previous sample.

A three-wire system consisting of two Py wires 20 nm thick, 100 nm wide, separated by a distance of 400 nm and bridged by an 80-nm-thick 100-nm-wide Cu strip. Between both Py wires, there is a third 100-nm-wide wire [Fig. 2(b)], consisting either of Cu (having a thickness of 80 nm), or a Py wire (having a thickness 20 nm), or there is no third wire.

A system consisting of two Py 20-nm-thick wires with different widths (200 nm width of injector and 100 nm width of detector), separated by 200 nm and bridged by a 250-nm-wide and 80-nm-thick Cu strip. In this device, we measured both DNLVS and difference of *local* voltage signal between the parallel and antiparallel state (DLVS) [Fig. 2(c)]. In the DLVS case, charge current flows through both Py wires.

In the following, we will discuss possible contributions coming from (i) surface scattering on Cu, $AR_{ss,Cu}$, (ii) surface scattering at Py/Cu interface $AR_{ss,Py/Cu}$, and (iii) interface nonpolarized resistance, $AR^*_{Py/Cu}$. The possible magnitude of each contribution has been determined to fit DNLVS for $w_{Cu}=100$ nm and then compared with other experimental data. All experimental data and calculated values are summarized in Table I.

(i) Surface scattering on Cu is introduced by a resistance $AR_{ss,Cu}$ short-cutting the up and down channels on the Cu surface. To decrease DNLVS for $w_{Cu}=100$ nm to experimental value, 0.7 mΩ, Cu surface scattering has to be $AR_{ss,Cu}=0.15\ f\Omega\ m^2$ (when surface scattering is assumed on both side sides and the top and bottom surface of a Cu wire) or $AR_{ss,Cu,side}=0.065\ f\Omega\ m^2$ (when surface scattering is assumed to be only on both sides of Cu). However, using those surface scattering resistances, the DNLVS calculated for the three-wire system (Table I) is too small compared with the experiment, showing that this contribution is not a dominant one.

(ii) and (iii) The properties of the Py/Cu interface are described by a presence of the interface layer, which has its own thickness t_I, spin-flip-length λ_I, conductivity σ_I, and spin-polarization γ_I.[22] However, the interface properties should not depend on t_I (this value is given *ad hoc* and is assumed as 1 nm in our calculations). Therefore, it is profitable to express interface properties by $\delta_I=t_I/\lambda_I$ and $AR^*_{Py/Cu}=t_I/\sigma_I$, which are independent on t_I.[22] The physical meaning of AR^* is clear: $2R^*(1-\gamma_I)$, $2R^*(1+\gamma_I)$ is a resistance of channel up, down and through the interface layer, respectively. As the physical meaning of δ_I is not so clear, we prefer to describe spin-flip scattering by interface scattering resistivity[20]

$$AR_s = AR^* \frac{4}{\delta \sinh \delta}, \tag{4}$$

which means a resistance short-cutting up and down channels on the interface.

To decrease DNLVS to experimental value at $w_{Cu}=100$ nm, different pairs of $AR^*_{Py/Cu}$, $AR_{s,Py/cu}$ can be used, as shown in Table I. When there is no interface resistance ($AR^*_{Py/Cu}=0$), then $AR_{s,Py/Cu}=2.6\ f\Omega\ m^2$. On the other hand, when $AR_{s,Py/Cu}=$inf then $AR^*_{Py/Cu}=15\ f\Omega\ m^2$. Both $AR_{s,Py/Cu}$ and $AR^*_{Py/Cu}$ contribute to the decrease of DNLVS.

Table I and Fig. 4(a) show that none of the combinations of pairs $AR^*_{Py/Cu}$, $AR_{s,Py/Cu}$ describes perfectly all experimental values; however, the agreement with all experimental data is within a factor of 2–3. Figure 4(a) shows that with increasing value of $AR^*_{Py/Cu}$, the difference between half and cross DNLVS is reducing, reflecting more homogeneous injection of j_{sp} over the Py-inj/Cu interface.

The most relevant interface properties are a pair of values $AR^*_{Py/Cu}=1\ f\Omega\ m^2$, $AR_{s,Py/Cu}=3.8\ f\Omega\ m^2$ ($\delta_{Py/Cu}=0.95$); as for this pair the mutual ratio between DNLVS's for a three-wire system (when the middle wire is Cu, Py, and nothing) agrees with the experiment. Then all calculated values for three-wire systems are about 1.8× larger than the experimental one. The disagreement by factor 1.8× can be related to a smaller value of λ_{Cu} than the expected 350 nm. The three-wire configuration with middle Py wire is particularly sensitive to $AR^*_{Py/Cu}$, as its value determines how large the amount of j_{sp} is absorbed by the middle Py wire.

Table I shows that the experimental value of DNLVS at $w_{Cu}=300$ nm is larger than the calculated one, particularly for cross configuration (experimental $DNLVS_{cross}=0.3$ mΩ, but calculated 0.14 mΩ). In another words, DNLVS (w_{Cu})

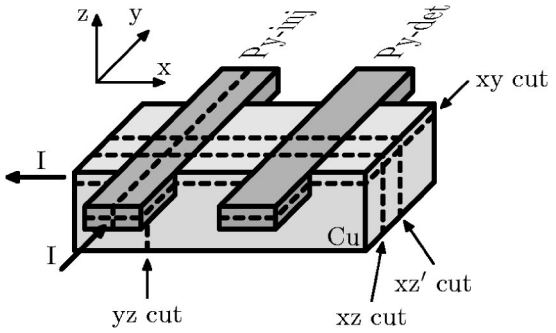

FIG. 8. The sketch of the device with indicated cut planes. The *yz*, *xz′* cuts are taken in the center of the Py injector, Cu wire, respectively. The *xy* cut is located 12.5 nm from device top, the *xz* cut is located 7.5 nm from the side of Cu wire.

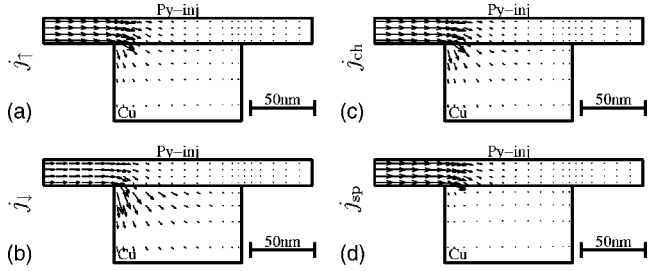

FIG. 9. The *yz* cut (defined in Fig. 8) of the current density of (a) current polarized up $j_\uparrow$, (b) current polarized down $j_\downarrow$, (c) charge current $j_{ch}=j_\uparrow+j_\downarrow$, and (d) spin-polarized current $j_{sp}=j_\uparrow-j_\downarrow$ in the device with $w_{Cu}=100$ nm with parallel magnetization. The length of arrow is proportional to value of a given current; this scaling is the same for all cuts.

decreases more slowly for the experiment than for the calculated value. It is probably due to the presence of a charge current j_{ch} at a position of the Py detector for wider w_{Cu}, as will be shown in Sec. IV B. The nonzero j_{ch} inside detector probably causes some additive contribution to DNLVS, either due to anisotropic magnetoresistance or to the scattering related with currents in plane i.e., currents flowing parallel with the Py/Cu interface.

Figure 4(b) also contains a dependence DNLVS(w_{Cu}) calculated from the model of Takahashi and Maekawa for $AR^*_{Py/Cu}=1$ fΩ m^2, $AR_{s,Py/Cu}=3.8$ fΩ m^2. We can see that there is a good agreement with 3D calculations. It shows when j_{sp} is homogeneous on the detector position, this model predicts a correct value of DNLVS.

The last part of Table I shows an agreement between experimental and calculated values of DNLVS and DLVS, determined for $w_{Cu}=250$ nm. We can see that for $AR^*_{Py/Cu}=1$ fΩ m^2, $AR_{s,Py/Cu}=3.8$ fΩ m^2, all experimental values are about twice as large compared to the calculated one. This can originate from anisotropic magnetoresistance or scattering related with in-plane currents, as already mentioned for DNLVS as $w_{Cu}=300$ nm.

Resistance $AR^*_{Py/Cu}=1$ fΩ m^2 is equal to the resistance of 48 nm of Cu or 7.3 nm of Py. Furthermore, interface scattering $AR_{s,Py/Cu}=3.8$ fΩ m^2 corresponds to scattering by Cu at a length of 950 and 2.5 nm inside Py [Eq. (4)]. The second value shows especially that interface scattering is not so large; however, it is enough to decrease DNLVS by one order of magnitude.

In conclusion of this section, we have shown that a major contribution to small DNLVS is due to interface scattering resistance $AR_{s,Py/Cu}$, short-cutting up and down channels at Py/Cu interfaces. The interface resistivity $AR^*_{Py/Cu}$ is also presented, but its contribution to the decrease of DNLVS is only a minor one. Such a large interface spin scattering has not been observed in Refs. 17 and 18. It can be related to two factors.

(1) The quality of our Py/Cu interface is lower than in Refs. 17 and 18. In our fabrication process, there are two steps which could decrease interface quality. On top of Py we deposited and removed photoresist to pattern Cu wire. Before Cu deposition, the surface was cleaned by Ar^+ bombardment and then the device was shortly taken out of vacuum to change the vacuum chamber. Notice that Jedema *et al.*[16] have used a very similar fabrication process as we did.

(2) The contribution of Py/Cu interface spin scattering is missing in previous works, investigating the Py/Cu system by means of magnetoresistivity ratio (MR).[17,18] Note that MR is sensitive to the value of j_{sp} passing free layer rather that to the value of spin accumulation $\Delta\mu$ at the position of free layer.[20] As we have shown,[20] the system can provide large MR (when large j_{sp} flows through free layer) although $\Delta\mu$ at the position of free layer can vanish. When $\Delta\mu$ vanishes, then short-cutting of up and down channels takes no effect and so interface spin scattering does not occur at the interface. In such a case, the MR (up to some limit) is insensitive to spin scattering on the free-layer/nonmagnetic-layer interface.

On the other hand, the nonlocal technique is particularly sensitive to $\Delta\mu$ at the detector/nonmagnetic-metal interface. When interface spin scattering is presented in this case, it

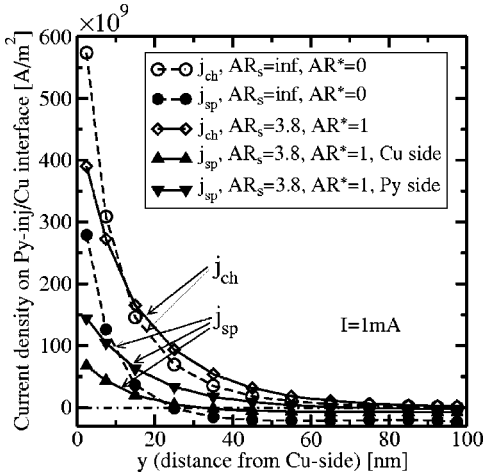

FIG. 10. The profiles of j_{ch} (open symbols) and j_{sp} (solid symbols) taken at the intersection of the Py injector/Cu interface and the *yz* cut (Fig. 8). The profiles were calculated for $w_{Cu}=100$ nm, for current I=1 mA, for $AR^*_{int}=0$, $AR_{s,Py/Cu}=$inf (circle), and for $AR^*_{int}=1$ fΩ m^2, $AR_{s,Py/Cu}=3.8$ fΩ m^2 (triangles and diamond). j_{sp} and j_{ch} are the same for parallel and antiparallel magnetizations. The symbols denote grid, for which the current densities are calculated.

significantly reduces DNLVS. Hence, it may be possible that small interface scattering is presented in both MR and nonlocal measurements, but did not take place in the case of MR measurements.

IV. CURRENT FLOWS INSIDE LATERAL SPIN-VALVE STRUCTURE

In this section we present in detail the current inhomogeneity inside a lateral spin-valve structure. Figure 8 shows a sketch of the device with indicated cut planes, on which the calculated current densities are presented in Figs. 9 and 11–13 and discussed in the following sections, Secs. IV A–IV C. The presented current densities were calculated for parallel magnetizations and for our best interface description $AR^*_{\mathrm{Py/Cu}}=1\ \mathrm{f}\Omega\ \mathrm{m}^2$, $AR_{\mathrm{s,Py/Cu}}=3.8\ \mathrm{f}\Omega\ \mathrm{m}^2$. For antiparallel magnetizations, we get very similar current flows as for the parallel one. This is in agreement with 1D models of nonlocal devices,[15,16] where current flows are exactly the same for parallel and antiparallel magnetic states.

A. Current description near Py injector

Figure 9 shows current density on the *yz* cut, which is taken in the center of the Py-injector wire (Fig. 8). Cuts (a)–(d) correspond to the cases for up and down current densities $j_\uparrow, j_\downarrow$, respectively, for charge current density $j_{\mathrm{ch}}=j_\uparrow+j_\downarrow$ and for spin-polarized current density $j_{\mathrm{sp}}=j_\uparrow-j_\downarrow$. All cuts show that the current is injected rather sharply through the Py-injector/Cu interface and then quickly spreads into the whole volume of Cu wire.

The values of j_{ch} and j_{sp} at the intersection of *yz* cut and Py-injector/Cu interface are presented on Fig. 10. The profile is shown for the device with $AR^*_{\mathrm{Py/Cu}}=0$, $AR_{\mathrm{s,Py/Cu}}=\mathrm{inf}$ (circles) and for $AR^*_{\mathrm{Py/Cu}}=1\ \mathrm{f}\Omega\ \mathrm{m}^2$, $AR_{\mathrm{s,Py/Cu}}=3.8\ \mathrm{f}\Omega\ \mathrm{m}^2$ (triangles and diamond). Due to spin-flip scattering on the interface, the j_{sp} flowing to the interface from the Py side (triangles down) is about twice larger than from j_{sp} outgoing the interface at Cu side (triangles up).

It is shown that both j_{ch} (open symbols) and j_{sp} (solid symbols) are sharply injected within the distance of 25 nm, 35 nm from the Py/Cu edge for $AR^*_{\mathrm{Py/Cu}}=1\ \mathrm{f}\Omega\ \mathrm{m}^2$, $AR_{s,\mathrm{Py/Cu}}=3.8\ \mathrm{f}\Omega\ \mathrm{m}^2$, and $AR^*_{\mathrm{Py/Cu}}=0$, $AR_{s,\mathrm{Py/Cu}}=\mathrm{inf}$, respectively. This different "length of injection" is only due to different values of $AR^*_{\mathrm{Py/Cu}}$, and is nearly independent on $AR_{s,\mathrm{Py/Cu}}$.When $AR^*_{\mathrm{Py/Cu}}$ is large then obviously the current is more spread over the interface and for tunnel contacts is can be considered as homogeneous. Furthermore, j_{sp} is positive only in the distance of 25 or 35 nm from the Py -injector/Cu edge, and then its value becomes negative. This means that in this region the injector reabsorbs a small part of the injected spin-polarized current, which decreases the spin-injection efficiency.

For different values of w_{Cu}, the length of injections is very similar to that presented in Fig. 10. It should be noticed that this sharp injection occurs in consequence of small Py conductivity, $\sigma_{\mathrm{Py}} \ll \sigma_{\mathrm{Cu}}$ and small thickness of Py wire $t_{\mathrm{Py}} < (w_{\mathrm{Cu}}, t_{\mathrm{Cu}})$. In other words, larger t_{Py} increases homogeneity of the injected current.

TABLE I. Experimental values of DNLVS (in mΩ) for various sample structures compared with values calculated by 3D models taking into account different processes decreasing DNLVS. Units of resistances are in $\mathrm{f}\Omega\ \mathrm{m}^2$, units of wire widths in nm. For details see Sec. III B 2.

	Experiment	$AR^*_{\mathrm{Py/Cu}}=0$, $AR_{\mathrm{s,Py/Cu}}=\mathrm{inf}$	$AR_{\mathrm{ss,Cu}}=0.15$	$AR_{\mathrm{ss,Cu,side}}=0.065$	$AR^*_{\mathrm{Py/Cu}}\approx 0$, $AR_{\mathrm{s,Py/Cu}}=2.6$ ($\delta_{\mathrm{Py/Cu}}\approx 0$)	$AR^*_{\mathrm{Py/Cu}}=0.3$, $AR_{\mathrm{s,Py/Cu}}=3.1$ ($\delta_{\mathrm{Py/Cu}}=0.6$)	$AR^*_{\mathrm{Py/Cu}}=1$, $AR_{\mathrm{s,Py/Cu}}=3.8$ ($\delta_{\mathrm{Py/Cu}}=0.95$)	$AR^*_{\mathrm{Py/Cu}}=3$, $AR_{\mathrm{s,Py/Cu}}=8.2$ ($\delta_{\mathrm{Py/Cu}}=1.1$)	$AR^*_{\mathrm{Py/Cu}}=15$, $AR_{\mathrm{s,Py/Cu}}\approx\mathrm{inf}$ ($\delta_{\mathrm{Py/Cu}}\approx 0$)
$\mathrm{DNLVS_{half}}$, $w_{\mathrm{Cu}}=100$	0.7	6.1	0.77	0.74	0.78	0.81	0.76	0.87	0.79
$\mathrm{DNLVS_{cross}}$, $w_{\mathrm{Cu}}=100$	0.62	6.06	0.75	0.73	0.76	0.79	0.75	0.87	0.79
$\mathrm{DNLVS_{half}}$, $w_{\mathrm{Cu}}=300$	0.6	3.1	0.66	0.87	0.49	0.47	0.40	0.40	0.29
$\mathrm{DNLVS_{cross}}$, $w_{\mathrm{Cu}}=300$	0.3	1.2	0.07	0.24	0.08	0.11	0.14	0.21	0.25
Three wires, no middle	0.25	3.72	0.034	0.032	0.45	0.47	0.46	0.54	0.48
Three wires, Cu middle	0.18	2.53	0.025	0.033	0.32	0.33	0.31	0.35	0.28
Three wires, Py middle	0.04	0.76	0.019	0.018	0.037	0.052	0.075	0.16	0.33
$\mathrm{DNLVS_{half}}$, $w_{\mathrm{Cu}}=250$	×	0.51	2.0	0.61	0.29	0.29	0.25	0.27	0.25
$\mathrm{DNLVS_{cross}}$, $w_{\mathrm{Cu}}=250$	0.4	1.3	0.20	0.33	0.12	0.14	0.15	0.21	0.24
$\mathrm{DLVS_{2Py}}$, $w_{\mathrm{Cu}}=250$	1	3.8	2.0	2.2	0.50	0.50	0.46	0.51	0.50
$\mathrm{DLVS_{1Py}}$, $w_{\mathrm{Cu}}=250$	0.4	2.4	1.7	1.8	0.34	0.32	0.28	0.29	0.26

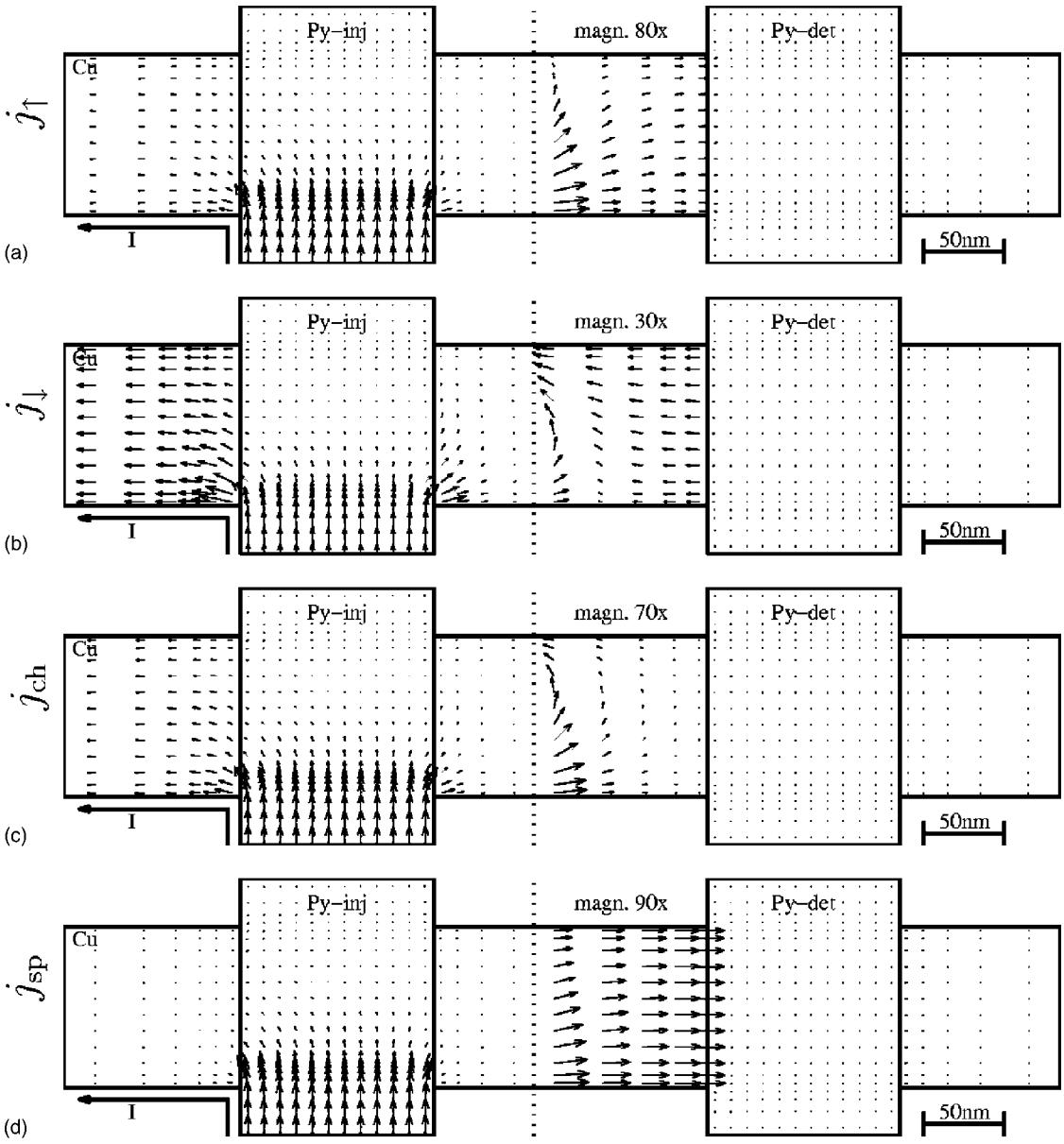

FIG. 11. The *xy* cut (defined in Fig. 8) of (a) $j_\uparrow$, (b) $j_\downarrow$, (c) j_{ch}, and (d) j_{sp} in the device with $w_{Cu}=100$ nm, parallel magnetization. The arrows have the same scaling for all cuts, and they are magnified on cut's right sides.

B. Top view on Cu

Figure 11 presents current density on the *xy* cut (defined in Fig. 8) taken at the depth of 12.5 nm from the top surface of the Cu wire. As already discussed, current is sharply injected at the Cu/Py-injector edge and hence $j_\uparrow$ and j_{sp} spread into the Cu wire from this edge [Figs. 11(a) and 11(d)].

Figure 11(d) also shows that for $w_{Cu}=100$ nm, j_{sp} at the position of the detector is fairly uniform in the *y* direction, i.e., in the direction parallel to the Py wire. When $j_\uparrow$ reaches the detector, it is successively spin scattered due to very short spin-diffusion length λ_{Py} and then current flows homogeneously back as $j_\downarrow$ [Figs. 11(a) and 11(b)].

Due to the sharp current injection, j_{ch} makes a whirl in the "diffusive" part of the Cu wire, where no charge current was expected [Fig. 11(c)]. In the present case ($w_{Cu}=100$ nm), the value of j_{ch} originating from this whirl at the detector position is negligible compared to j_{sp}. However, when $\ell_{Cu} < w_{Cu}$ (ℓ_{Cu} being distance between Py wires), then $j_{ch} \gtrapprox j_{sp}$ at detector position. This can be seen in Fig. 12(a) for $w_{Cu}=300$ nm. Figure 12(b) shows that also j_{sp} for $w_{Cu}=300$ nm is inhomogeneous at detector position, having maximal value at one side of Cu/Py-detector interface. This explains different values between cross and half configurations.

C. Current description near Py detector

Figure 13 presents current density on the *xz* cut (defined in Fig. 8) which is taken 7.5 nm from the side of the Cu wire. Figure 13(a) shows that the flow of $j_\uparrow$ into the detector is also inhomogeneous and is dominant at the side of the Py-detector/Cu, which is close to the injector. As already mentioned above, due to very short spin-diffusion length

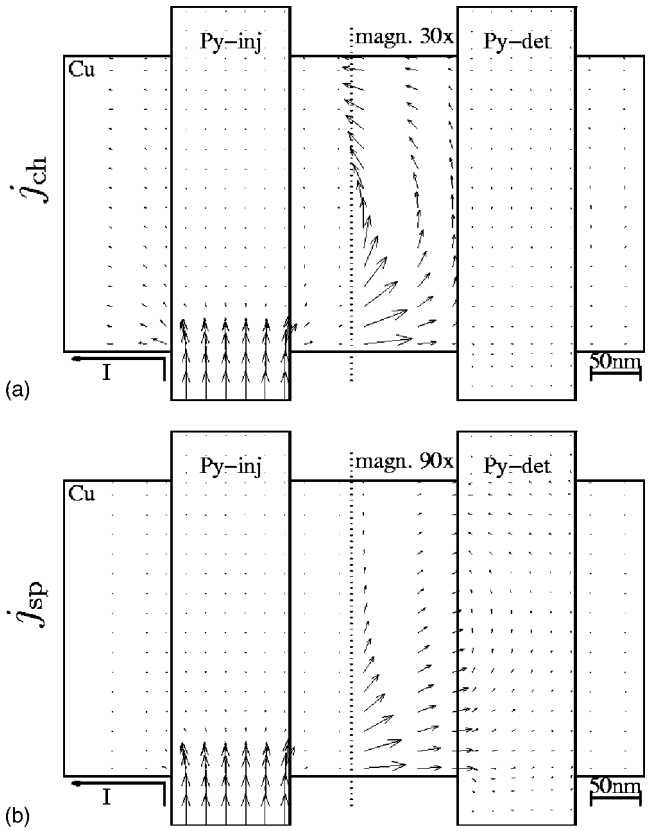

FIG. 12. The *xy* cut (defined in Fig. 8) of (a) j_{ch} and (b) j_{sp} in the device with $w_{Cu}=300$ nm. The arrows have the same scaling for both cuts, and they are magnified on cut's right sides.

$\lambda_{Py}=4.3$ nm, $j_\uparrow$ flowing into the detector is immediately reversed inside the Py detector and coming back as $j_\downarrow$ [Fig. 13(b)]. This can be understood as a resistance shunting (or "short-cutting") the up and down channels. This also explains the behavior of j_{sp} [Fig. 13(d)], whose flow is absorbed by the detector.

Figure 14 shows j_{ch} and j_{sp} on the intersection between the Py-detector/Cu interface and xz' cut (defined in Fig. 8),

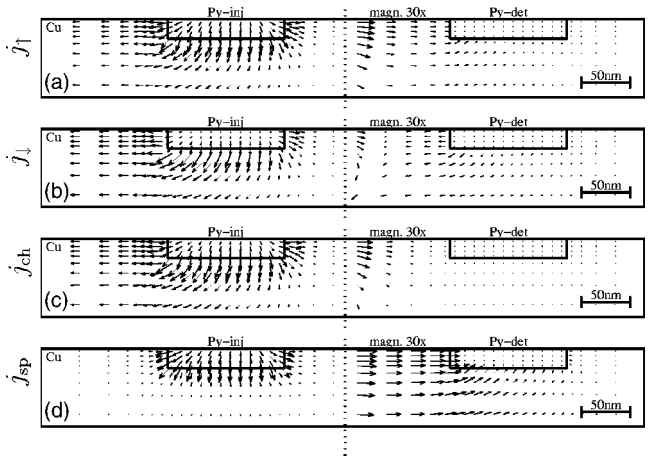

FIG. 13. The *xz* cut (defined in Fig. 8) of (a) $j_\uparrow$, (b) $j_\downarrow$, (c) j_{ch}, and (d) j_{sp} in the device with $w_{Cu}=100$ nm, parallel magnetization. The arrows have the same scaling for all cuts, and they are magnified on cut's right sides.

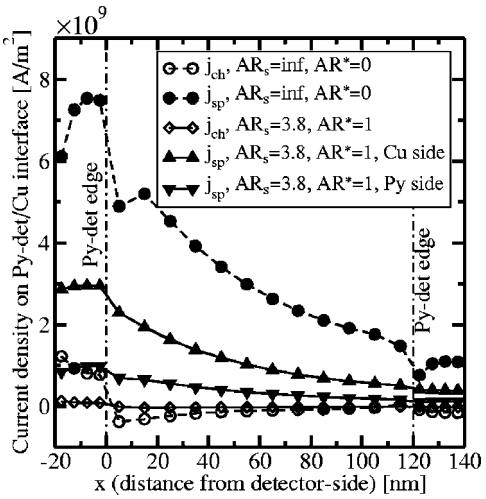

FIG. 14. The profile of j_{ch} and j_{sp} on the intersection of the Py-detector/Cu interface and the xz' cut (defined in Fig. 8) for parallel magnetization state. The rest as in Fig. 10.

which is taken at the center of Cu wire. The vertical dash-dot lines show the position of edges inside the Py-detector wire embedded in the Cu wire, i.e., ranges $x\in(-20,0)$ and $x\in(120,140)$ correspond to the side part of the Py wire, although the range $x\in(0,120)$ represents the bottom part of the Py detector wire. We can see that both j_{sp} and j_{ch} are inhomogeneous, decaying approximately exponentially with $1/e$ decrease length 80 nm. This decay is mainly the result of the competition between Cu conductivity σ_{Cu} and spin-flip scattering inside the Py and Py/Cu interface.

When the interface resistances $AR^*_{Py/Cu}=1$ fΩ m^2, $AR_{s,Py/Cu}=3.8$ fΩ m^2 are introduced, j_{sp} flowing to the detector is decreased (and hence DNLVS is decreased), as can be seen in Fig. 14. Due to the presence of $AR_{s,Py/Cu}$, the current flowing to the interface from the Cu side (triangle up) is about $3\times$ larger than one outgoing to the injector (triangle down). Hence, 2/3 of j_{sp} entering the detector are short cut, absorbed by an interface.

There is also j_{ch} at the Py-detector/Cu interface, having a value about 10% of j_{sp}. The j_{ch} originates because $j_\uparrow$ and $j_\downarrow$ are injected to and/or ejected from the Py detector at a slightly different position, i.e., j_{ch} has negative value around $x\gtrsim 0$ and positive at $x\lesssim 0$. It means that part of $j_\uparrow$ current, which is injected to the Py detector from the side of the Py wire, is ejected as $j_\downarrow$ from its bottom part.

V. CONCLUSION

We have fabricated lateral spin-valve devices consisting of the Permalloy (Py) and Cu wires. We have observed that the difference of the nonlocal voltage signal (DNLVS) between parallel and antiparallel magnetization has different values for half and cross configurations. The difference between these two configurations increases when the width of the Cu stripe increases.

To understand the observed behavior in detail, we have developed formalism calculating spatial (3D) distribution of the spin-polarized current and electrochemical potential in-

side the device. We found that the current distribution inside the lateral spin-valve device with ohmic contact is a rather complex interplay between geometry and electrical properties of all the involved materials.

Despite those large current inhomogeneities, the DNLVS calculated from our 3D model are in a good agreement with 1D model given by Takahashi et Maekawa.[15] However, both 1D and 3D predicts about 10× larger DNLVS than experimental values. We have attributed the smallness of DNLVS to interface scattering resistance $AR_{s,\mathrm{Py/Cu}}=3.8\ \mathrm{f}\Omega\ \mathrm{m}^2$ ($\delta_{\mathrm{Py/Cu}}=0.95$) short-cutting up and down channels at the Py/Cu interface. On one hand, this value of $AR_{s,\mathrm{Py/Cu}}$ decreases DNLVS by a factor of 10. On the other hand, it corresponds only to scattering which occurs inside Py at a distance of 2.5 nm. When this interface scattering resistance can be reduced, DNLVS may be enhanced significantly. The fact that such an interface resistivity has not been observed before[17,18] may be related either to a lower quality of our interface or to insensitivity of MR to small surface scattering in some cases.

Interface resistance $AR^{*}_{\mathrm{Py/Cu}}=1\ \mathrm{f}\Omega\ \mathrm{m}^2$ is also presented at the Py/Cu interface, but its contribution to smallness of DNLVS is minor. The value of this resistance mainly modifies the j_{sp} inhomogeneity in the structure. Using this description of the Py/Cu interface, we found agreement with all our experimental data (local and nonlocal voltage signals measured on systems with two or three Py wires) within a factor of 2.

The current is injected from the Py injector to Cu sharply, within the distance of 30 nm. Part of the injected spin-polarized current is reabsorbed by the injector itself. Current flow over the Py-detector/Cu interface is also inhomogeneous, having the largest value on the side of the Py detector close to the injector and decaying approximately exponentially with a $1/e$ decrease within the distance 80 nm.

[1] *Spin electronics*, edited by M. Ziese and M. Thornton (Springer, Berlin, 2001).
[2] I. Zutic, J. Fabian, and S. Das Sarma, Rev. Mod. Phys. **76**, 1 (2004).
[3] A. Brataas, Y. Tserkovnyak, G. E. W. Bauer, and B. I. Halperin, Phys. Rev. B **66**, 060404(R) (2002).
[4] G. E. W. Bauer, Y. Tserkovnyak, D. Huertas-Hernando, and A. Brataas, Phys. Rev. B **67**, 094421 (2003).
[5] M. Johnson, J. Appl. Phys. **75**, 6714 (1994).
[6] M. Johnson, Phys. Rev. Lett. **70**, 2142 (1993).
[7] A. Fert and S. F. Lee, Phys. Rev. B **53**, 6554 (1996).
[8] F. J. Jedema, B. J. van Wees, B. H. Hoving, A. T. Filip, and T. M. Klapwijk, Phys. Rev. B **60**, 16 549 (1999).
[9] F. J. Jedema, A. T. Filip, and B. J. van Wees, Nature (London) **410**, 345 (2001).
[10] F. J. Jedema, H. B. Heersche, A. T. Filip, J. J. A. Baselmans, and B. J. van Wees, Nature (London) **416**, 713 (2002).
[11] J. A. Katine, F. J. Albert, R. A. Buhrman, E. B. Myers, and D. C. Ralph, Phys. Rev. Lett. **84**, 3149 (2000).
[12] P. C. van Son, H. van Kempen, and P. Wyder, Phys. Rev. Lett. **58**, 2271 (1987).
[13] T. Valet and A. Fert, Phys. Rev. B **48**, 7099 (1993).
[14] S. Takahashi and S. Maekawa, Phys. Rev. Lett. **88**, 116601 (2002).
[15] S. Takahashi and S. Maekawa, Phys. Rev. B **67**, 052409 (2003).
[16] F. J. Jedema, M. S. Nijboer, A. T. Filip, and B. J. van Wees, Phys. Rev. B **67**, 085319 (2003).
[17] S. Dubois, L. Piraux, J. M. George, K. Ounadjela, J. L. Duvail, and A. Fert, Phys. Rev. B **60**, 477 (1999).
[18] S. Steenwyk, S. Hsu, R. Loloee, J. Bass, and W. Pratt, Jr., J. Magn. Magn. Mater. **170**, L1 (1997).
[19] P. Holody, W. C. Chiang, R. Loloee, J. Bass, W. P. Pratt, Jr., and P. A. Schroeder, Phys. Rev. B **58**, 12 230 (1998).
[20] J. Hamrle, T. Kimura, T. Yang, and Y. Otani, cond-mat/0409309 (unpublished).
[21] T. Kimura, J. Hamrle, Y. Otani, K. Tsukagoshi, and Y. Aoyagi, Appl. Phys. Lett. **85**, 3501 (2004); **85**, 5382 (2004).
[22] W. Park, D. Baxter, S. Steenwyk, I. Moraru, W. Pratt, Jr., and J. Bass, Phys. Rev. B **62**, 1178 (2000).